Improved performance of highly multiplexed silicion-on-insulator microring sensor chips by surface structure implementation

Sam Werquin[a,b], Diedrik Vermeulen[c], Arne Goes[d], Anabelle Van Eeghem[e,b], Peter Dubruel[e,b] and Peter Bienstman[a,b]

[a]Department of Information Technology (INTEC), Ghent University-imec, B-9000 Ghent, Belgium;
[b]Center for Nano- and Biophotonics (NB-Photonics), Ghent University, B-9000 Ghent, Belgium;
[c]Acacia Communications, 3601 Route 36, Hazlet, NJ 07730, USA;
[d]Agrosafve NV, Technologiepark 4 (Bio-incubator), B-9052 Zwijnaarde, USA, Belgium;
[e]Polymer Chemistry and Biomaterials Group, Ghent University, Krijgslaan 281 (S4), B-9000 Ghent, Belgium

ABSTRACT

Silicon-on-insulator microring resonators have proven to be an excellent platform for label-free nanophotonic biosensors. The high index contrast of the silicon-an-insulator platform allows for fabrication of micrometer size sensors and a high degree of multiplexing. To enable robust, low-noise performance of a microring resonator sensor chip in a lab-on-a-chip setting, flood illuminating an array of vertical grating couplers is a promising approach to couple input light into the chip. This technique provides a very high alignment tolerance while at the same time exciting multiple sensors simultaneously for rapid parallel read-out. We demonstrate this technique to obtain a highly multiplexed chip output combined with real time sensor information. However, parasitic reflections on the chip surface can deteriorate the sensor signal and limit the performance. We investigate the use of surface structures to limit these parasitic signals and show a significant improvement of the sensor operation.

Keywords: photonic biosensor, interference, grating.

1. INTRODUCTION

Silicon-on-insulator (SOI) microring resonators have proven to be an excellent platform for label-free nanophotonic biosensors.[1–3] The high index contrast of SOI allows for fabrication of micrometer-size ring resonators used for a variety of photonic applications.[4] Their small size makes microring resonators excellent candidates for highly multiplexed assays[5] in biosensing applications. The high index contrast of the SOI platform causes high confinement of the optical fields in the waveguides, which makes the microrings very sensitive to changes on the waveguide surface.[6] This explains their very high sensitivity to biomaterials. Low-noise performance of microring resonators is a mandatory requirement for medical applications. In a lab-on-a-chip setting, this has to be combined with ease of use and robustness against a variety of external disturbances. Rather than coupling light into the microchip waveguides using traditional fiber coupling techniques[7] which require delicate allignment and micrometer accuracy, we make use of a collimated laser beam to illuminate the chip surface. This improves robustness against vibrations and allows for simultaneous excitation of a compact grating coupler array for better multiplexing possibilities.[8] In this paper, we demonstrate real time interrogation of 64 microring sensors simultaneously. However, various reflections from the SOI deteriorate the sensor performance. Improved

Further author information: (Send correspondence to S.W.)
S.W.: E-mail: sam.werquin@intec.ugent.be
D.V.: E-mail: Diedrik.Vermeulen@acacia-inc.com
A.G.: E-mail: arne.goes@agrosavfe.com

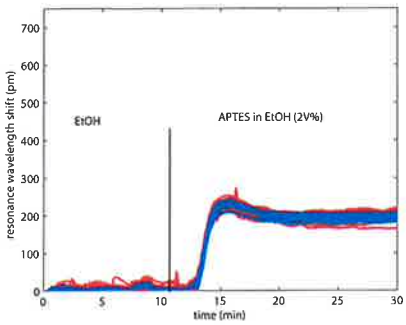

Figure 1: The recorded binding curve during the silanization of the surface. Individual sensor response signals are plotted. Red curves show the drop sensors and pass sensor signals are plotted in blue. A baseline is established by flowing ethanol over the sensors. After 10 minutes the APTES solution is introduced to the sensors. An average resonance wavelength shift of 200 pm is recorded by 47 sensors.

grating couplers for photonic applications[9,10] have been suggested. But parasitic transmission paths through the chip substrate still form an important limitation of the sensor performance in biosensing applications. Here, we develop an integrated anti-transmission grating that enhances the performance of the biosensors. Simulation results and experimental demonstrations are reported.

2. MICRORING RESONATOR SENSOR ARRAY

A Santec TSL-510 tunable laser source generates the input signals. We use a collimated laser beam to illuminate 4 input fiber couplers simultaneously. The light is coupled to waveguides on the SOI chip where it is distributed to different ring sensors using 3dB multimode interference splitters. This allows us to adress an array of 64 microring sensors with a single input optical fiber. The array consists of a combination of all-pass and drop sensors. The output waveguides of the sensors are routed to a fiber coupler array, where the output signals are recorded by a Xenics Xeva 1.7-320 infrared camera. Using the techniques described in,[8] microfluidic channels are integrated on the chip surface. The channels are designed to guide an analyte over the chip surface to the different sensors of the sensing array. Technological limitations on the channel dimensions imply we can only adress 3 out of 4 sensors of the matrix. All sensors will light up, but only those located in the channels are in contact with the analyte and will monitor the reaction when molecules bind to the chip surface.

2.1 Multiplexed detection with real time binding information

We use the microring sensor array to monitor the silanization of the silicon surface by tracking the change in resonance wavelength of the microring sensors. After processing the data recorded from the infrared camera, this results in the real time binding curve of figure 1. Because they do not provide any useful information, the sensors that are not in contact with the analyte are not included in this graph. Out of the 48 active sensors, only one did nog light up on the output camera. All 47 remaining sensor signals are shown in figure 1. During the first 10 minutes of this experiment, the chip channels are filled with ethanol to establish the baseline signal. After approximately 10 minutes, the ethanol is replaced by a 2 volume percent solution of aminopropyltrietoxysilane (APTES) in ethanol. The silanization of the silicon surface is apparent by the resonance wavelength shift of the microring sensors. A positive shift indicates the deposition of a higher refractive index material on the surface. After switching back to ethanol, a residual shift of approximately 200 pm is recorded. This indicates the formation of a permanent silane layer on the silicon surface. This silanization is recorded in real time by 47 sensors simultaneously. The standard deviation of the response of all sensors during silanization is only 9 pm.

2.2 Complementary DNA sequence detection

The same microring resonator chip in a similar setup has also been used to detect a 25 base-pair complementary DNA sequence. For the chemical preparation of the silicon chip surface, we follow the procedure described in.[2] The surface modification is finalized by the covalent bonding of a 25 base-pair DNA capture probe to an active

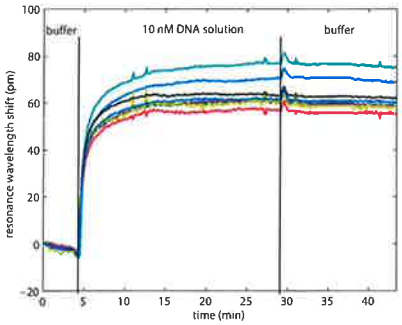

Figure 2: The recorded binding curve during the complementary DNA sequence detection. Individual sensor response signals are plotted. A baseline is established by flowing hybridization buffer over the sensors. After 5 minutes, the 10 nM complementary DNA solution is introduced to the sensors. 30 minutes into the experiment, the liquid is switched back to the original buffer solution. An average resonance wavelength shift of 74 pm is recorded.

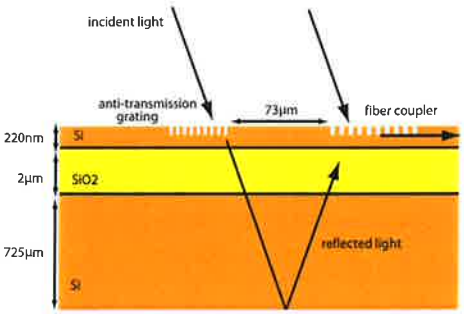

Figure 3: Schematic representation of light incident on chip surface. Light coupling to the waveguide through the fiber coupler after reflection on the substrate induces an interference pattern. An anti-transmission grating can be implemented to block this parasitic light path.

hydrazine linker. During the detection experiment, we record the signals from 8 sensors. The changing resonance wavelength of the microring resonators provides real time information about to binding of the complementary DNA strand. The detection step is performed in a hybridization buffer of 50 volume-percent formamide in PBS (0,01 M) pH 7.4 to facilitate hybridization. A concentration of 10 nM is chosen for the complementary strand solution. The resulting binding curve of the complementary DNA detection experiment is depicted in figure 2. Note that this graph has been corrected for a bulk shift that occurres when switching from the pure hybridization buffer to the hybridization buffer with complementary DNA solution. The permanent resonance wavelength shift amounts to 74 pm on average.

These successful experiments demonstrate the potential of using robust illumination by collimated laser light for real time multiplexed detection experiments with a SOI microring resonator array. However, the illumination of the chip surface by a collimated laser beam also has some significant drawbacks, as various reflections deteriorate the sensor performance. To tackle these problems, the following sections will describe an approach to limit the parasitic interferences due to reflections of the back substrate.

3. SURFACE GRATING STRUCTURES

Fig. 3 shows a schematic representation of the incident light and the layered microchip surface. The chip is processed from a Smart-Cut SOI wafer[11] and consists of a thick silicon substrate, a 2 μm thick oxide buffer layer and a 220 nm silicon top layer. It is in this top silicon layer that integrated photonic structures such as microring sensors are patterned. The chip surface is illuminated by a collimated light beam. Part of the light is incident

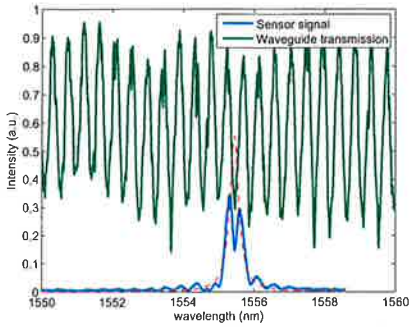

Figure 4: Transmission signals disturbed by interference due to parasitic reflections. The dashed line shows the undisturbed sensor signal

on a fiber coupler[12] in the waveguide and couples directly into the photonic wire waveguide with high efficiency. However, light incident on the chip surface in the area in front of this grating will be transmitted through the silicon-air interface. This beam propagates through the chip substrate and reflects at the back surface. As the longitudinal component of the wavevector is conserved upon refraction, the Bragg condition (1) for the fiber coupler is also met by the reflected light beam.

$$\beta = k_{in} \sin(\theta) + K \tag{1}$$

In (1), $\beta = \frac{2\pi}{\lambda} n_{eff}$ is the propagation constant of the guided mode and $K = \frac{2\pi}{\Lambda}$, with Λ the period of the grating. $k_{in} = \frac{2\pi}{\lambda}$ is the wave vector and θ is the angle between the incoming light and the surface normal. The reflected light will then couple efficiently from the burried oxide layer to the waveguide. The round trip through the chip substrate introduces a significant path length difference and affects the phase of the reflected light. The phase difference between the directly coupled and the reflected light generates a strong interference pattern in the transmitted power of microchip and the microring sensors signals as demonstrated in fig. 4.

This pattern has a period of 450 pm and modulates the microring drop signals to an extent that the peak intensity is greatly suppressed and the sensor signal is effectively destroyed. This can also be seen from fig. 4. Experimental characterization of the chip thickness confirms that reflections of the back surface generate an interference pattern with the observed period. Even in the case the microring signal is not completely destroyed, the interference pattern can still severely deteriorate sensing operation. During the detection of a biomolecule, the change in refractive index at the surface of the biosensor induces a shift in wavelength visible in the sensor signal. However, the strong modulation signal does not shift. This gives rise to highly undesirable features in an experimentally recorded binding curve and could lead to false detection events. Therefore, we suggest an integrated solution that can be implemented with the same lithographic procedure used for the definition of the transducer and thus does not require any additional processing steps. We implement anti-transmission grating structures at the chip-air interface in the position that leads to the parasitic light path, as shown in fig. 3. This limits the transmission efficiency and reduces the intensity of the reflected light. Other techniques, like local metal deposition to absorb the parasitic light yield similar results, but this requires alterations to the chip processing. We will show that our approach efficiently reduces the parasitic reflected signals and their corresponding interference pattern.

4. SIMULATIONS

Using 2D-FDTD simulations, we have investigated the feasability of two different implementations for the anti-transmission grating of fig. 3. A first approach uses a backward coupling grating (BCG) to diffract light to the waveguide in the opposite direction. This light will then propagate away from the fiber coupler rather than refracting to the substrate region. Using a taper structure, the backward propagating light is dissipated in the silicon slab region that covers the chip surface. The grating is realized by etching 70 nm deep lines in the 220 nm thick waveguide layer, with a duty cycle of 50%. For light with a wavelength of 1550 nm and an incidence angle of 10°, the Bragg condition implies a grating period of 540 nm for the backward coupling grating.

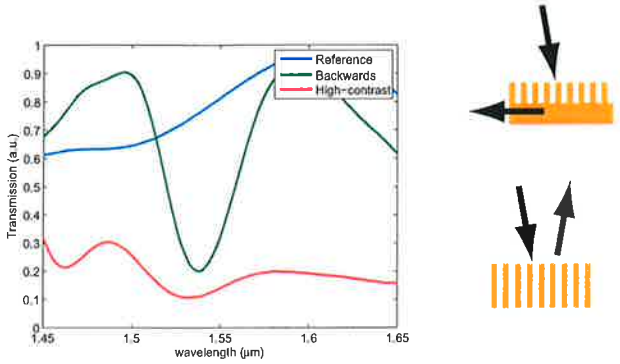

(a) (b)

Figure 5: (a) Simulated transmission to the substrate for different grating implementations. Introduction of the surface gratings significantly reduces the transmitted power. (b) FIB-crossection with schematic representation of light propagation for backward (top) and high contrast grating (bottom).

Alternatively, we have also investigated the implementation of a high contrast grating (HCG). Instead of guiding the light to the slab region, the HCG prevents light from reaching the fiber coupler by maximizing the first order reflection. This type of grating has been primarily investigated for the applications in vertical cavity surface emitting lasers (VCSELs) because of its high reflection over wide wavelength bands and relatively large fabrication tollerances.[13,14] The high contrast is obtained by etching 220 nm deep lines through the full height of the waveguide layer. Fig. 5 shows the simulated transmission to the substrate for the reference situation and after implementation of the gratings. These simulations clearly show a significant reduction of the transmitted power after processing the gratings on the chip surface. A fundamental difference between both approaches also becomes apparent. The backward coupling grating is only efficient in a narrow band around the design wavelength of 1550 nm, whereas the HCG can introduce high reflection over a relatively wide wavelength band. As described in,[15] more complex simulation methods can be used to further optimize the HCG design.

5. EXPERIMENTS

Based on the simulation results, a design combining the fiber couplers and the anti-transmission gratings has been fabricated in a CMOS-pilot line at imec. For a chip thickness of 725 μm, the location of the gratings on the surface is calculated to be 73 μm in front of the fiber coupler. In this position, the designed gratings will prevent the incident light to be transmitted to the back of the substrate and reflected up to the fiber coupler. This eliminates the parasitic interferences. The chip is mounted on a measurement chuck for characterization. A collimated laser beam illuminates the input fiber couplers and the surrounding chip surface. The tunable laser is swept at 5 nm/s over a 20 nm range with a wavelength resolution of 10 pm. An IR-camera is used to record the output spectra with a framerate of 500 Hz.

5.1 Results

Fig. 6a shows the recorded spectrum for a fiber coupler combined with the BCG with grating period of 530 nm. Around 1551.5 nm, a region with reduced interference effects is clearly visible. This suppression region corresponds to the grating wavelength targeted during design. The data is analysed by Fourier transforming the spectrum. This provides more insight into the origin of the oscillations. Fig. 6c compares the Fourier spectrum of a 3 nm region around 1551.5 nm to that of a 3 nm region with maximum interference strength. This shows the dominant component corresponding to oscillations with a 450 pm period is succesfully suppressed in the 1551.5 nm region. The suppression region shows the occurance of a new Fourier component corresponding to 220 pm period oscillations, but with significantly lower intensity. This component can be attributed to second order reflections of the chip substrate. Indeed, light incident on the chip surface 146 μm in front of the fiber coupler will make two round trips through the substrate, reflecting twice off the bottom surface and thus arriving at the fiber coupler with lower intensity and giving rise to less pronounced interference effects. Fig. 6b and 6d

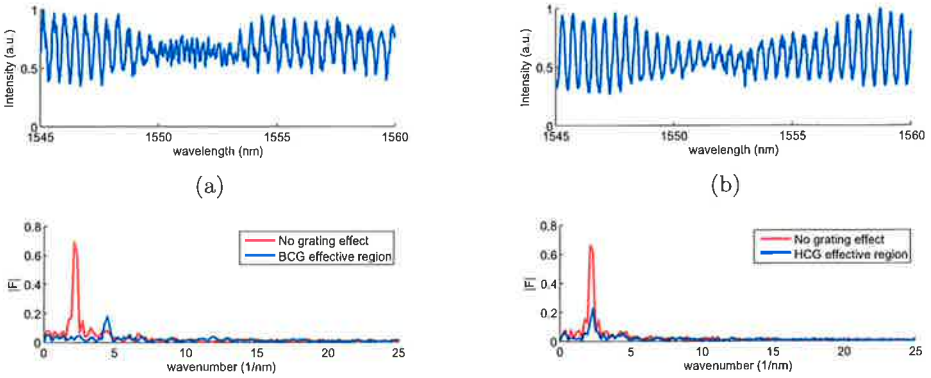

Figure 6: Transmission spectra of fiber coupler combined with BCG (a) and HCG (b). The grating effective region is clearly visible in both cases. (c) and (d) show the comparison of the Fourier spectrum in and outside the grating region of effect for BCG and HCG, respectively. The dominant Fourier components are significantly reduced in both cases.

show the results for a HCG implemented $73\,\mu m$ in front of the fiber coupler. The period of the high contrast grating is 1050 nm. Here, the 450 pm period remains the dominant oscillation, while its strength is significantly reduced. A small component at 220 pm can barely be discerned from noise.

5.2 Discussion

The intensity pattern in the signal waveguide can be modeled as a simple two beam interference signal given by

$$I = I_1 + I_2 + 2\sqrt{I_1 I_2}\cos(\Delta\phi) \tag{2}$$

Here I_1 is the intensity of the light coupling directly into the waveguide through the fiber coupler, I_2 is the intensity of the light coupling in the waveguide via reflections on the backside and $\Delta\phi$ accounts for the path length difference between both interfering waves. As the Fourier components from Fig. 6c and fig. 6d originate from the only oscillating term of (2), they are proportional to the amplitude of the cosine, or $2\sqrt{I_1 I_2}$. Comparing two Fourier spectra provides us with a means to determine the reduction in intensity of the parasitic beam I_2 as a consequence of the implementation of the surface grating structures. The intensity reduction or grating suppression efficiency is given by

$$10\log_{10}\left[\left(\frac{X_1}{X_2}\right)^2\right] \tag{3}$$

Here, X_1 and X_2 are the amplitude of the dominant Fourier components outside, respectively inside the grating's spectral region of effect. For the BCG, the signal originating from second order reflections becomes dominant in the suppressed region while the 450 pm component is completely suppressed. Therefore, the strength of the Fourier component corresponding to 220 pm period oscillations should be used for X_2 in expression (3). For the HCG, the 450 pm component remains dominant, so X_2 corresponds to the Fourier component of this period. This results in an efficiency of 12 dB for the backward coupling grating and an efficiency of only 10 dB for the high-contrast reflection grating. The obtained efficiencies are only representative for the grating effect around the central grating wavelength. To obtain a spectral representation of the grating efficiency, a different model can be applied. The strength of the interference pattern is also apparent in the extinction ratio of consecutive fringes. From (2), the dependence of the ratio I_1/I_2 on the extinction ratio is analytically calculated to be

$$\sqrt{I_1/I_2} = \frac{(1-x)}{-(1+x)+\sqrt{4x}} \tag{4}$$

with x the intensity ratio between consecutive maxima and minima of the spectrum. The result is plotted in fig. 7, both for the backward coupling grating and the high-contrast grating.

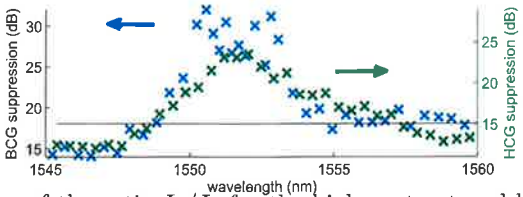

Figure 7: Wavelength dependency of the ratio I_1/I_2 for the high-contrast and backward coupling grating. The suppression threshold is indicated by a line. A higher maximum suppression is obtained for the BCG, but the HCG is effective over a wider wavelength range.

Outside the grating effective region, we can determine a baseline level. Without grating effect, I_2 is found to be 12 to 15 dB weaker than the intensity of light coupling directly into the waveguide. We experimentaly find an extinction due to the backward coupling grating up to 27 dB, or 12 dB higher than the baseline. Here, we have to keep in mind that this number is limited by second-order reflections of the chip substrate. The direct transmission through the grating is practically completely eliminated, as suggested by the Fourier spectrum. If we set an arbitrary suppression threshold to an additional extinction of 3 dB, the bandwidth of the suppressed region is 6 nm, with a 4 nm region that exceeds 10 dB suppression. For the high-contrast reflection grating, we calculate a reduction of the intensity I_2 up to 24 dB, or a suppression of 11 dB. The maximum suppression is reduced compared to the BCG, but the suppression threshold is exceeded over a wider range, i.e. 8 nm. As the free-spectral range of the microring sensors is 4 nm, we can always find a microring resonance inside the suppression regions. Notice the suppression efficiencies obtained from the spectral representation correspond very well to values calculated from the Fourier components. The difference between simulation and experiment for the HCG can be attributed to the simulation model, which is less suited for describing the very fast phase changes in the high-contrast region and the design parameters are not accurately predicted. The results discussed in this paragraph suggest the backward coupling grating as the best solution for the interference problem. If this grating is repeated in the position leading to the second order reflections, additional performance improvements are expected. However, after optimization of the high-contrast grating through more complex simulations, we expect they can eventually outperform the backward coupling grating, especially because of their reduced wavelength dependence.

6. CONCLUSION

For ease of use, the fragile fiber-chip interface should be avoided in lab-on-a-chip applications. Instead, a collimated laser beam can be used for a robust coupling method with high alignment tolerance. In this paper, we have demonstrated multiplexed detection with sensor array of up to 64 sensors. Using microfluidic packaging, we have shown real time silanization of the silicon surface and complementary DNA sequence detection by recording the resonance wavelength shift of part of the sensor array. We point out the negative effect parasitic reflections can have on the microring resonator response and suggest a straightforward technique to reduce these parasitic reflections. We demonstrate that implementing suppression gratings to block parasitic lightpaths through the substrate efficiently reduces the interferences, without additional processing steps. In particular, a high contrast reflection grating and a grating that diffracts incoming light in the backwards propagation direction of the waveguide are investigated. A suppression efficiency up to 12 dB is obtained for the backward coupling grating.

Acknowledgment

The authors would like to acknowledge the Special Research Fund of Ghent University (BOFUGent), the FP7 project CanDo and the Innovative Medicines Initiative (RAPP-ID project, grant agreement, no. 115153).

REFERENCES

[1] De Vos, K. D., Bartolozzi, I., Schacht, E., Bienstman, P., and Baets, R., "Silicon-on-Insulator microring resonator for sensitive and label-free biosensing," *Optics express* **15**(12), 7610–7615 (2007).

[2] Qavi, A. J. and Bailey, R. C., "Multiplexed detection and label-free quantitation of microRNAs using arrays of silicon photonic microring resonators.," *Angewandte Chemie (International ed. in English)* **49**, 4608–11 (June 2010).

[3] Qavi, A. J., Mysz, T. M., and Bailey, R. C., "Isothermal Discrimination of Single-Nucleotide Polymorphisms via Real-Time Kinetic Desorption and Label-Free Detection of DNA Using Silicon Photonic Microring Resonator Arrays.," *Analytical chemistry* **83**, 6827–33 (Sept. 2011).

[4] Bogaerts, W., Heyn, P. D., Vaerenbergh, T. V., Vos, K. D., Kumar, S., Claes, T., Dumon, P., Bienstman, P., Thourhout, D. V., and Baets, R., "Silicon Microring Resonators," *Laser & Photonics Reviews* **6**(1), 47–73 (2011).

[5] Iqbal, M., Gleeson, M. A., Spaugh, B., Tybor, F., Gunn, W. G., Hochberg, M., Baehr-Jones, T., Bailey, R. C., and Gunn, L. C., "Label-Free Biosensor Arrays Based on Silicon Ring Resonators and High-Speed Optical Scanning Instrumentation," *IEEE Journal of Selected Topics in Quantum Electronics* **16**(3), 654–661 (2010).

[6] Luchansky, M. S., Washburn, A. L., Martin, T. a., Iqbal, M., Gunn, L. C., and Bailey, R. C., "Characterization of the evanescent field profile and bound mass sensitivity of a label-free silicon photonic microring resonator biosensing platform.," *Biosensors & bioelectronics* **26**, 1283–1291 (July 2010).

[7] Roelkens, G., Vermeulen, D., Selvaraja, SHalir, R., Bogaerts, W., and Thourhout, D. V., "Grating-Based Optical Fiber Interfaces for Silicon-on-Insulator Photonic Integrated Circuits," *IEEE J. Quantum Electron.* **17**(3), 571–580 (2011).

[8] De Vos, K., Girones, J., Claes, T., De Koninck, Y., Popelka, S., Schacht, E., Baets, R., and Bienstman, P., "Multiplexed Antibody Detection With an Array of Silicon-on-Insulator Microring Resonators," *IEEE Photonics Journal* **1**, 225–235 (Oct. 2009).

[9] Li, Y., Vermeulen, D., De Koninck, Y., Yurtsever, G., Roelkens, G., and Baets, R., "Compact grating couplers on silicon-on-insulator with reduced backreflection.," *Optics letters* **37**, 4356–8 (Nov. 2012).

[10] Vermeulen, D., Koninck, Y. D., Li, Y., Lambert, E., Bogaerts, W., Baets, R., and Roelkens, G., "Reflectionless grating couplers for Silicon-on-Insulator photonic integrated circuits," *Optics express* **20**(20), 1919–1921 (2012).

[11] Aspar, B., Bruel, M., Moriceau, H., Maleville, C., Poumeyrol, T., Papon, A., Claverie, A., Benassayag, G., Auberton-Herve, A., and Barge, T., "Basic mechanisms involved in the smart-cut(r) process," *Microelectronic Engineering* **36**(1), 233–240 (1997).

[12] Van Laere, F., Roelkens, G., Ayre, M., Schrauwen, J., Taillaert, D., Van Thourhout, D., Krauss, T. F., and Baets, R., "Compact and Highly Efficient Grating Couplers Between Optical Fiber and Nanophotonic Waveguides," *JOURNAL OF LIGHTWAVE TECHNOLOGY* **25**(1), 151–156 (2007).

[13] Huang, M. C., Zhou, Y., and Chang-Hasnain, C. J., "A surface-emitting laser incorporating a high-index-contrast subwavelength grating," *Nature Photonics* **1**, 119–122 (Feb. 2007).

[14] Zhou, Y., Huang, M. C. Y., and Chang-Hasnain, C. J., "Large Fabrication Tolerance for VCSELs Using High-Contrast Grating," *IEEE Photonics Technology Letters* **20**, 434–436 (Mar. 2008).

[15] Karagodsky, V., Sedgwick, F. G., and Chang-Hasnain, C. J., "Theoretical analysis of subwavelength high contrast grating reflectors.," *Optics express* **18**, 16973–88 (Aug. 2010).

PROCEEDINGS PAPER • NEW

Improved performance of highly multiplexed silicion-on-insulator microring sensor chips by surface structure implementation

Author(s): Sam Werquin; Diedrik Vermeulen; Arne Goes; Anabelle Van Eeghem; Peter Dubruel; Peter Bienstman

FORMAT	MEMBER PRICE	NON-MEMBER PRICE
PDF	**$15.00**	**$18.00**

Paper Abstract

Silicon-on-insulator microring resonators have proven to be an excellent platform for label-free nanophotonic biosensors. The high index contrast of the silicon-an-insulator platform allows for fabrication of micrometer size sensors and a high degree of multiplexing. To enable robust, low-noise performance of a microring resonator sensor chip in a lab-on-a-chip setting, flood illuminating an array of vertical grating couplers is a promising approach to couple input light into the chip. This technique provides a very high alignment tolerance while at the same time exciting multiple sensors simultaneously for rapid parallel read-out. We demonstrate this technique to obtain a highly multiplexed chip output combined with real time sensor information. However, parasitic reflections on the chip surface can deteriorate the sensor signal and limit the performance. We investigate the use of surface structures to limit these parasitic signals and show a significant improvement of the sensor operation.

Paper Details

Date Published: 20 February 2014
PDF: 8 pages
Proc. SPIE 8954, Nanoscale Imaging, Sensing, and Actuation for Biomedical Applications XI, 89540O (20 February 2014); doi: 10.1117/12.2037266

Published in SPIE Proceedings Vol. 8954:
Nanoscale Imaging, Sensing, and Actuation for Biomedical Applications XI
Alexander N. Cartwright; Dan V. Nicolau, Editor(s)

© SPIE. Terms of Use

Back to Top